

Non-local, diamagnetic electromagnetic effects in long MITLs

E. G. Evstatiev,^{1,*} M. H. Hess,¹ and N. D. Hamlin¹

¹Sandia National Laboratories, Albuquerque, New Mexico 87185

(Dated: August 23, 2024)

We identify the physics responsible for the critical reduction of current losses in magnetically insulated transmission lines (MITLs) before magnetic (self-) insulation has been established. Focusing on time-dependent physics, a drive current with a prototypical sine squared temporal profile introduces sufficiently strong time dependence that steady state results alone become insufficient for the complete understanding of current losses. We find that the effects of time dependence are most pronounced in *long* MITLs, i.e., MITLs in which an electromagnetic wave traverses its length in time comparable to the current pulse length. The time-dependent physics can be described as non-local, diamagnetic electromagnetic response of space charge limited currents. As the length of the MITL is reduced (in the above sense), current losses converge to those based on the well known Child-Langmuir law in static external fields. We present a simple one-dimensional (1D) model that encapsulates the essence of this physics. We find excellent agreement with 2D particle-in-cell (PIC) simulations for two MITL geometries, Cartesian parallel plate and azimuthally symmetric straight coaxial. Based on the 1D model, we explore various scaling dependencies of current losses with relevant parameters, e.g., peak current, peak pulse time, geometrical dimensions, etc. We also propose an improved physics model of magnetic insulation, which could help improve predictions of current losses by common circuit element codes, such as BERTHA. Lastly, we describe how to calculate temperature rise due to electron impact, as a diagnostic within the 1D model.

Keywords: magnetically insulated transmission line; MITL; parallel plate; coaxial; magnetic insulation; non-local; diamagnetic; particle-in-cell; PIC; kinetic; space charge limited; SCL; electron emission; BERTHA; circuit element model; Z machine.

I. INTRODUCTION

Pulsed power devices [1–3] require the transport of large amounts of power over relatively long distances. Previous experiments [4–6] have shown that 80% or more of the input energy can be delivered to a load up to 10 m away from a generator. At Sandia National Laboratories’ Z machine, up to 40 terawatts of power is delivered from the stack to a load over more than a meter distance, with little losses. At the heart of the ability to transport such large amounts of power is the physics of magnetic insulation (also called self-insulation) in magnetically insulated transmission lines (MITLs) [7–11].

During the beginning of the current pulse, electron emission from the cathode is observed when the electric fields exceed values of about 20–30 MV/m [5]. These electrons may or may not be initially insulated, something highly dependent on MITL geometry and temporal current pulse profile. For the prototypical sine squared current pulse shape used throughout this work,¹ uninsulated electrons are typically observed in *long* MITLs, i.e., MITLs in which an electromagnetic (EM) wave traverses its length in time comparable to the length of the current pulse itself. The longer the MITL, the longer the time

interval of uninsulated emission. Uninsulated electrons may contribute significantly to current loss and anode temperature rise and are for this reason a major concern when designing long MITLs.

Current losses are being predicted in one of two ways. First, fully kinetic electromagnetic particle-in-cell (PIC) simulations are considered as the most general and trusted approach [12–17]. By its nature, the PIC method [18, 19] is very computationally expensive. For this reason, approximate one-dimensional (1D) circuit element models (CEM) have been devised [20–24]. Since CEM models are only 1D, their computational cost is many orders of magnitude lower than that of PIC, and for this reason are preferred for preliminary MITL design, leaving PIC simulations for final verification. Both methods have shown reliable predictions of current losses in time-dependent settings (i.e., using current pulses), implying that they both capture the essential physics.

In this work we propose an alternative one dimensional method based on electromagnetic fields and sources instead of circuit elements. One may consider such a formulation as the basis for the circuit element method. Working with the fields and sources has the advantages that (i) one can interpret the results in a physically intuitive way; and (ii) a more direct comparison with electromagnetic PIC simulations is possible. The latter is important in the verification of preliminary MITL designs.

The main assumptions of our one dimensional model are these:

(A-i) Infinitely small anode-cathode (AK) gap; i.e., AK gap that is much smaller than all other MITL dimensions. This assumption allows us to decouple

* eevsta@sandia.gov (corresponding author)

Copyright (2024) E. G. Evstatiev, M. H. Hess, and N. D. Hamlin. This article is distributed under a Creative Commons Attribution-NonCommercial-NoDerivs 4.0 International (CC BY-NC-ND) License.

¹ The conclusions in this work also hold for more realistic current pulses used on Z , however, we do not show results for such pulses.

the 2D problem into two 1D problems. It also assumes that changes of (local in space) space charge limited (SCL) currents are instantaneous, i.e., we neglect the time for electrons to cross the AK gap;

- (A-ii) SCL currents vary according to the well known Child-Langmuir law [25, 26];
- (A-iii) The magnetic insulation ramps down SCL currents smoothly, according to a *Hull curve*.²

In the main exposition, we consider a parallel plate Cartesian geometry, which allows for a certain degree of analytical treatment. The straight coaxial geometry with a finite AK gap can also be treated analytically; however, its treatment greatly simplifies in the small AK gap limit, for which we outline some detail in Appendix A.

The paper is structured as follows. Section I is an introduction. Section II introduces the reduced 1D electromagnetic model. Section III describes the non-local, diamagnetic time-dependent effects in long MITLs. Section IV presents scaling of MITL losses with various parameters. Section V presents a model for magnetic insulation, improving upon a similar such in CEM models. Section VI presents the temperature rise diagnostics within the 1D model. Section VII summarizes and presents final concluding remarks.

II. A ONE-DIMENSIONAL ELECTROMAGNETIC MODEL OF A MITL

In the geometry under consideration, all electromagnetic waves, external and emitted by SCL currents, propagate as TEM modes. We choose z as the propagation direction, x as the transverse (AK gap) direction, then y is the ignorable direction (symmetry dimension). Correspondingly, the non-trivial components of the fields and currents (current densities) are E_x , B_y , and j_x . Quantities also depend on time, t . Waves are launched at $z = 0$ in the positive z -direction. Waves propagating in the negative z -direction (to the left) are absorbed at $z = 0$. There is a perfectly conducting load (short) at the opposite end of the MITL, $z = L$, so that waves are reflected off that end.

The basic model of SCL emission assumes that a local SCL current is “once-on-always-on.” In other words, we assume that once the threshold for SCL emission is exceeded at a particular location and instant of time, the inventory of plasma is sufficient to supply any amount of electrons necessary to sustain zero electric field at the cathode at maximal SCL current; this is the typical assumption in PIC as well. Some models assume initially a

source-limited emission, which later transitions into SCL emission. We do not include such detail as it does not qualitatively affect the following discussion and results.

As already mentioned, the small AK gap assumption allows us to decouple the two spatial dimensions of the problem. The two 1D problems consist of an electromagnetic problem along the direction of EM wave propagation and an electrostatic problem in the direction across the AK gap. First, let us consider the electromagnetic part of the model. Suppose a spatial location z_0 starts emitting SCL current at time $t_0 = 0$. This emission model can be mathematically represented as a Dirac delta-function in space and a Heaviside step-function in time

$$j_x(z, t) = I_0 \delta(z - z_0) \theta(t), \quad (1)$$

with current I_0 per unit length (unit length in the ignorable y -direction). We assume I_0 to be the current *on the conductor*. The relation between the current in the AK gap and the current on the conductor is illustrated in Fig. 1. We also note that the delta function has dimensions of inverse length while the step function is dimensionless; thus j_x has the dimensions of current density, e.g., Ampere/m² in SI units.

Working in the Coulomb gauge, the equation for the electromagnetic waves can be reduced to the wave equation for the vector potential

$$\frac{\partial^2 A_x(z, t)}{\partial z^2} - \frac{1}{c^2} \frac{\partial^2 A_x(z, t)}{\partial t^2} = -\mu_0 j_x(z, t) \quad (2)$$

with electric and magnetic fields given by

$$E_x(z, t) = -\frac{\partial A_x(z, t)}{\partial t}, \quad (3)$$

$$B_y(z, t) = (\nabla \times \mathbf{A})_y = \frac{\partial A_x(z, t)}{\partial z}. \quad (4)$$

Using the fundamental solution (Green’s function) of the wave operator (d’Alembertian), $\partial_t^2 - c^2 \partial_z^2$, in one spatial dimension (of infinite z -extent), $\mathcal{E}_1 = \frac{1}{2c} \theta\left(t - \frac{|z|}{c}\right)$, we follow the general rule for finding the special solution of Eq. (2) by convolution [27], $A_x(z, t) = \mathcal{E}_1 \star (c^2 \mu_0 j_x)$. The integrals are easy to evaluate and give

$$A_x(z, t) = \frac{I_0 Z_0}{2} \left(t - \frac{|z - z_0|}{c} \right) \theta \left(t - \frac{|z - z_0|}{c} \right), \quad (5)$$

where ϵ_0 and μ_0 are the permittivity and permeability of vacuum, $Z_0 = \sqrt{\mu_0/\epsilon_0} \approx 376.7 \Omega$ is the vacuum (free space) impedance, and c is the speed of light in vacuum. The fields following from Eqs. (3), (4) are

$$E_x(z, t) = -\frac{I_0 Z_0}{2} \theta \left(t - \frac{|z - z_0|}{c} \right), \quad (6)$$

$$B_y(z, t) = -\text{sign}(z - z_0) \frac{E_x(z, t)}{c}. \quad (7)$$

² We use this term in the hope that there is no confusion with a similar one used in the published literature.

Note that the magnetic field has a discontinuity at the current location, $z = z_0$, since this is a surface (sheet) current. The jump across the discontinuity is the difference between the values on the right and on the left of the current sheet, and gives the expected result

$$[B_y]_{z=z_0} = B_y(0^+) - B_y(0^-) = \frac{I_0 Z_0}{c} = \mu_0 I_0. \quad (8)$$

An external (vacuum) field can be launched into the MITL by setting up a current source at the launch side of the MITL, say $z_0 = 0$, with a desired temporal dependence. For example, a sine squared current pulse peaking at value I_{peak} at time $t = \tau_{\text{peak}}$ can be set up by

$$j_x(z, t) = -I_{\text{peak}} \delta(z) \sin^2 \left(\frac{\pi t}{2\tau_{\text{peak}}} \right). \quad (9)$$

The corresponding fields can be calculated by following the steps leading to Eq. (5):

$$E_x^{\text{ext}}(z, t) = \frac{I_{\text{peak}} Z_0}{2} \sin^2 \left(\frac{\pi(t - |z|/c)}{2\tau_{\text{peak}}} \right), \quad (10)$$

$$B_y^{\text{ext}}(z, t) = \frac{E_x(z, t)}{c}, \quad (11)$$

where the magnetic field sign corresponds to a wave launched in the positive z -direction. Our numerical implementation indeed uses Eq. (9) to launch external waves into the MITL.

Now consider the dynamics within the AK gap. At any instant of time, we assume the SCL current is given by Child-Langmuir's law,

$$j_x(z, t) \equiv j_{\text{CL}} = \frac{4\epsilon_0}{9d^2} \sqrt{\frac{2e}{m}} V(z, t)^{3/2}, \quad (12)$$

where d is the size of the AK gap, e and m are the charge and mass of the electron, and $V(z, t)$ is calculated from the electric field Eq. (6) as follows. Within the AK gap, we know from the steady state Child-Langmuir law (see for example [28]) that at any given z and t

$$V(x; z, t) = V_0 \left(\frac{x}{d} \right)^{4/3}, \quad (13)$$

where $x = 0$ is the cathode and $x = d$ is the anode. The semicolon in the list of arguments in Eq. (13) emphasizes the fact that z and t are here considered as parameters, not actual arguments to V . At the anode, the *total* electric field is the sum of the external (electromagnetic) field (6) and the space charge field:

$$E_x^{\text{tot}}(x = d) = - \left. \frac{dV(x)}{dx} \right|_{x=d} = - \frac{4}{3} \frac{V_0}{d}.$$

We now identify the value of the electric potential at the anode at any z and t with the voltage at the anode, $V_0 = V(z, t) = -E_x(z, t) d$. This gives the potential determining the value of the current $j_x(z, t)$ in Eq. (2),

$$j_x(z, t) = \frac{4\epsilon_0}{9d^2} \sqrt{\frac{2e}{m}} [E_x(z, t) d]^{3/2}, \quad (14)$$

completing the system of equations (2)–(4). (Absolute values are taken whenever necessary.)

The total electric field at the anode is given by

$$E_x^{\text{tot}}(x = d; z, t) = \frac{4}{3} E_x(z, t), \quad (15)$$

from which

$$V_0 = V(z, t) = \frac{3}{4} E_x(z, t) d. \quad (16)$$

We use equations (15) and (16) in two cases. First, in the 1D code output, we augment the electric field found from Eq. (6) by 4/3, according to Eq. (15), at any location where *uninsulated* SCL emission has initiated. For definiteness, we compare fields and currents between models near the anode. And second, relation (16) is instrumental to correctly determine the Hull curve from PIC simulations, as discussed in Sec. V.

As a final comment in this section, we note that the simulation of SCL emission by PIC has both physical and numerical aspects. The physical aspect is that of the Child-Langmuir law. In emission due to field stress, after a certain threshold value of the (normal) electric field has been exceeded, electrons are emitted from the cathode and conduct space charge limited current in the anode-cathode gap, when uninsulated. The numerical aspect aims to implement an algorithm that uses computational particles and finite time steps, that is numerically stable, and that produces results in agreement with the physical aspect. In this regard, “numerical knobs” exist in PIC codes which, if not used carefully, may noticeably distort the results. For example, Sandia’s PIC code EMPIRE [29], implements a function that ramps up SCL current in time from a small fraction to its full value according to some functional dependence. A similar capability exists in CHICAGO [17, 30–32]. We believe that most PIC codes allow for similar numerical knobs. Accordingly, we have implemented a similar parameter our 1D electromagnetic model, allowing for a closer comparison of the results. We refer the reader to the extensive literature for more detail (e.g., [18, 33–35], with a brief discussion also given in Ref. [36]).

III. NON-LOCAL, DIAMAGNETIC ELECTROMAGNETIC EFFECTS OF SCL CURRENTS

We observe from Eqs. (6), (7) that in a long MITL, a wave emitted by a local SCL current per the “once-on-always-on” rule propagates throughout the full length of the MITL with *undiminished amplitude*, i.e., is *nonlocal*. The *diamagnetic* nature of the waves can be seen from Fig. 1. The figure also shows the correspondence between the SCL current within the volume of the MITL, \mathbf{j}_{SCL} , and the changes in the currents on the electrodes, namely, $I_0 = j_{\text{SCL}}/2$. We discuss these two effects below.

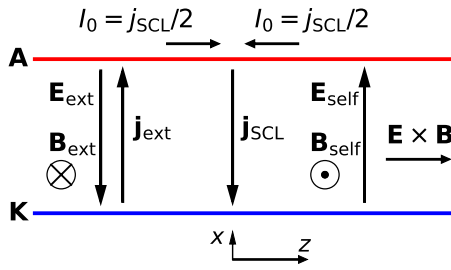


FIG. 1. Directions of fields and currents within the MITL and on the conductor. Currents with subscript '0' denote current on the conductor. The field directions are shown only for waves propagating in the positive z -direction; waves propagating to the left have reversed magnetic field direction. Both self-waves are thus diamagnetic.

The non-local effect of SCL currents is demonstrated in Fig. 2, where the temporal evolution of a wave from a point current source at $z = 50$ cm with $I_0 = 100$ kA is shown [cf. Eq. (1)]. The current source indicated in the figure is in the negative x -direction, hence, the fields have opposite signs to those in Eqs. (6), (7). The MITL has a length of $L = 1$ m and an AK gap $d = 5$ mm. At $t = 0.5$ ns, two waves are seen propagating away from the source (directions are indicated by arrows) and before reflection from the short at $z = 1$ m. At $t = 2.5$ ns, the right-propagating wave has reflected and is now propagating to the left, while the left-propagating wave has exited the MITL. It is seen that since the amplitudes of the waves due to this source are non-diminishing in time and in space (up to the wave front), after reflection the electric field of the right-propagating wave cancels out exactly the electric field of the reflected (now left-propagating) wave so that the total electric field behind the reflected wave is exactly zero. The magnetic fields of the incoming and outgoing waves *add* and at $t = 5.5$ ns a steady state has been established with only a constant magnetic field present in the MITL. The jump in the magnetic field can be calculated from Eq. (8) and equals $[B_y]_{z=50\text{ cm}} \simeq 0.126$ T. In a time-dependent system (time-dependent current source), the emitted and reflected waves would not cancel exactly due to the temporal delay between the time of emission and the time the reflected wave has traveled back to the source, at which time the emitted wave from the source will have changed its amplitude. Note that this relatively low current (peak currents of interest in the Z machine are 20–30 MA, while smaller pulsed power machines have currents of order mega-ampere) already generates an electric field with amplitude $\simeq 19$ MV/m, which is very close to the threshold for SCL emission discussed in the Introduction. Conversely, currents of this magnitude may be expected during the beginning of SCL emission.

The large diamagnetic response of the SCL currents is demonstrated in Fig. 3 at three times, 6.5 ns, 9 ns, and 24 ns. For this setup, we use a sine squared drive current pulse with $I_{\text{peak}} = 20$ MA and $\tau_{\text{peak}} = 100$ ns. SCL emis-

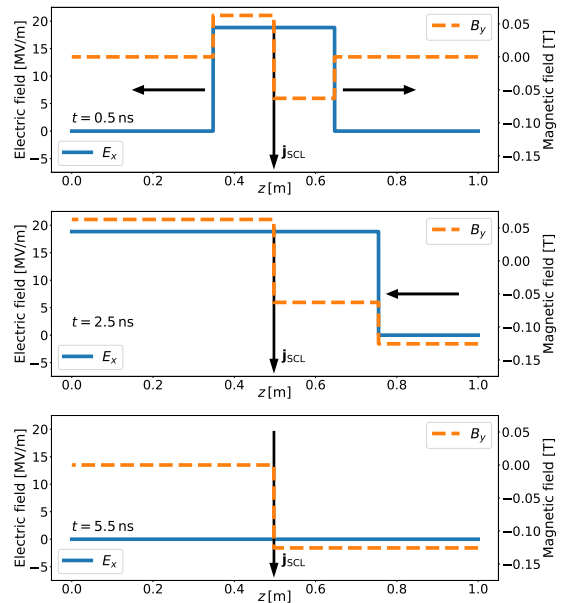


FIG. 2. Time evolution of a wave emitted from a point source with a step function time dependence, Eq. (1). Top panel: two waves propagating away from the current source and before reflection from the load. Middle panel: the right-propagating wave after reflection is now propagating to the left, the left-propagating wave has exited the system. Bottom panel: steady state after the EM waves have left the MITL.

sion starts at about 5 ns. In about 1.5 ns, the electric field measured near the anode has *accumulated* an amplitude comparable to the threshold for SCL emission, 24 MV/m (top panel). The middle panel of the figure shows the diamagnetic wave after reflection from the conducting short at $z = 1$ m. The bottom panel shows the electromagnetic fields after magnetic insulation, which approach the vacuum field values (black dash-dotted lines). The similarity between the fields in Figs. 3 and 2 is obvious with the difference that in the time-dependent case, the large diamagnetic EM field is generated by an SCL current that has *accumulated* in time (and is spread out in space).

Another typical consequence of the diamagnetic effect is shown in Fig. 4, where current densities at the anode along the extent of the MITL are shown. Non-zero SCL current densities are also an indication of where the SCL emission threshold has been exceeded. The top panel shows that in about 1.5 ns of (uninsulated) SCL emission, about 30 cm of cathode (surface) extent has started emitting according to the PIC model and about 35 cm in the 1D model. At time 9 ns, shown in the bottom panel, since the diamagnetic EM fields subtract from the vacuum fields, the total resulting electric field in the remaining part of the MITL extent ($\gtrsim 30$ cm) has fallen below the emission threshold, halting SCL emission almost completely for the next 3 ns. The vacuum fields at 9 ns are shown in the middle panel of Fig. (3) and suggest that without this diamagnetic effect, SCL emission

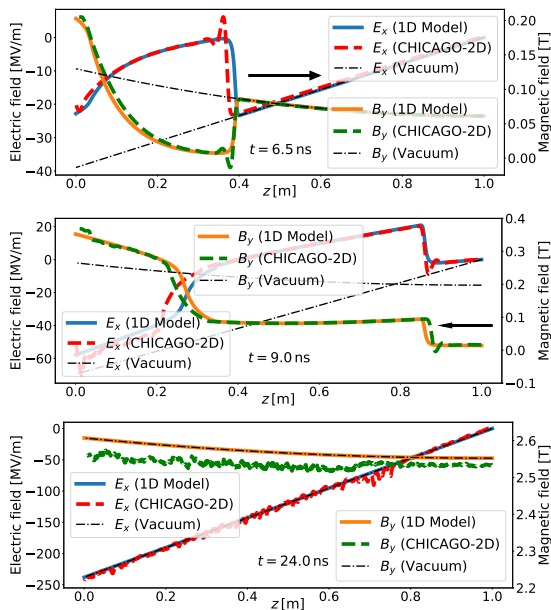


FIG. 3. Time evolution of the electric and magnetic fields in an SCL simulation. Top panel: the initial diamagnetic electromagnetic wave emitted by initial SCL currents, at 6.5 ns. Middle panel: The diamagnetic wave after reflection from the conducting load, at 9 ns. Bottom panel: electromagnetic fields after magnetic insulation approaching the vacuum (external) fields, at 24 ns.

would have initiated in $\sim 0\text{--}60$ cm of the cathode surface.

This dynamics of fields and currents tends to repeat itself and thus the emitting fraction of MITL surface grows in “jumps” instead of gradually, as one might expect from a smooth temporal drive. In other words, for the time interval before the full cathode surface starts emitting (this is roughly the time for the first diamagnetic wave to reach the load), there is a sequence of a propagating SCL current pulse followed by a pause. During the propagating part of the cycle, the diamagnetic effect accumulates until the external wave’s amplitude falls below the SCL emitting threshold. During the pause part of the cycle, the external fields grow sufficiently to eventually overwhelm the diamagnetic effect.

We see that the non-local diamagnetic response acts to lower the magnitude of SCL currents and reduce current losses in two ways. First, by limiting the extent of emitting surface. This effect varies in magnitude in various setups, however, it can be used as a telltale sign of the non-local, diamagnetic response of SCL currents. And second, by lowering the SCL current within the emitting surface (recall $j_{\text{SCL}} \sim E^{3/2}$). This effect is *bi-directional* since local SCL currents emit diamagnetic EM waves in both propagating directions. The result of this is observed in Fig. 4 (bottom panel) where the current density near the launch side ($z = 0$) has been greatly reduced, forming a sharp peak near $z \simeq 30$ cm. It is the combination of these two effects that results in dramatically lower overall current losses in long MITLs compared to

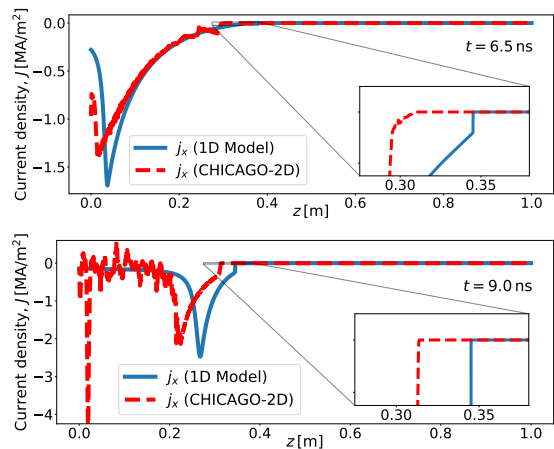


FIG. 4. Time evolution of the loss current density. Top panel: loss current density profile at 6.5 ns. Bottom panel: loss current density profile at 9 ns. It is seen that the peak of the loss current density propagates at about $0.65c$, however, the insets of the two panels show that SCL emission is inhibited past about 0.3 m in CHICAGO or 0.35 m in the 1D simulation. The latter phenomenon is quite common and is a result of the non-local diamagnetic EM effects by SCL currents.

SCL emission in vacuum fields alone (see also the discussion of Fig. 5 below).

Some interesting observations can relate our results to previous work. First, the peak of the uninsulated current density propagates about 23 cm in 1.5 ns, which is approximately at the speed of $0.65c$. The current pulse observed (on the conductor) in the MITL is the difference between the vacuum current and the loss current, and it would therefore appear that the main current pulse propagates at that speed as well. Second, since the SCL (loss) current is seen to have a sharp peak, the main current pulse would exhibit “front sharpening.” Both features have been previously reported by experimental and numerical work [4, 5, 37]. On the other hand, the “jump-like” propagation discussed above has not been previously reported.

IV. SCALING STUDIES OF MITL LOSSES BASED ON THE 1D ELECTROMAGNETIC MODEL

We have tested relatively extensively the validity of the 1D model against PIC simulations, varying parameters such as MITL dimensions (length, AK gap), peak current, pulse length, as well as threshold for SCL emission within relevant ranges. In very short MITLs, for example, lowering E_{th} to artificially low values is necessary in order to observe uninsulated SCL emission.

We define current loss as

$$I_{\text{loss}}(t) = \int_0^L dz j_{\text{SCL}}(z, t) \quad (17)$$

where $j_{\text{SCL}}(z, t)$ is the *uninsulated* current and note that

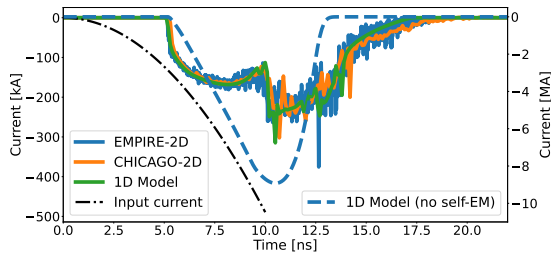


FIG. 5. Current loss vs. time: Comparison between the 1D model and 2D PIC simulations with EMPIRE and CHICAGO (left-hand scale). The dashed blue curve (right-hand scale) shows the current loss without accounting for non-local diamagnetic effects.

it is a function of time alone. A comparison of predicted current loss by the 1D model as well as EMPIRE and CHICAGO 2D PIC is shown in Fig. 5 (left-hand scale). We note the excellent agreement between all three codes. The input current pulse (without SCL emission) is indicated with a dash-dotted black line. Also plotted in Fig. 5 is the loss current (by the 1D model) based on only the Child-Langmuir law in vacuum fields (right-hand scale), i.e., without accounting for diamagnetic EM fields emitted by SCL currents. We see that such a prediction, even for a 1 m long MITL, is grossly inaccurate, with a maximum current loss of over 8 MA compared to the expected 250 kA. (The fact that in this case the loss current exceeds the input current should be no cause for alarm. It is an artifact of the simulation setup used throughout this work, where we use a feed of infinite source of energy. Using such a feed removes unnecessary complications due to variations in the input drive current and allows for a clean demonstration of the physics under consideration.)

In this section we look at some scaling laws that could suggest appropriate MITL design parameters and provide additional insight into the time-dependent effects in long MITLs. We would like to compare a quantity that characterizes MITL losses in both space and time. For this purpose, we find it convenient to define the *loss charge* as

$$Q_{\text{loss}} = \int_0^{t_{\text{ins}}} dt I_{\text{loss}}(t), \quad (18)$$

and the time integral is until the time t_{ins} of complete magnetic insulation along the MITL; then Q_{loss} is the total charge collected by the anode. We normalize this to the total charge delivered by the drive current, which for a sine squared pulse equals $Q_{\text{tot}} = I_{\text{peak}}\tau_{\text{peak}}$.

In Fig. 6 (a) we show the scaling of MITL losses with the AK gap distance, d , for three different lengths. The pulse has $I_{\text{peak}} = 20$ MA and $\tau_{\text{peak}} = 100$ ns. We observe that for small AK gap sizes, $Q_{\text{loss}}/Q_{\text{tot}}$ scales as a power law $\sim 1/x$ while for larger gap sizes that scaling does not hold. In practical applications, small gap sizes are usually preferred and then the $\sim 1/x$ scaling can be used.

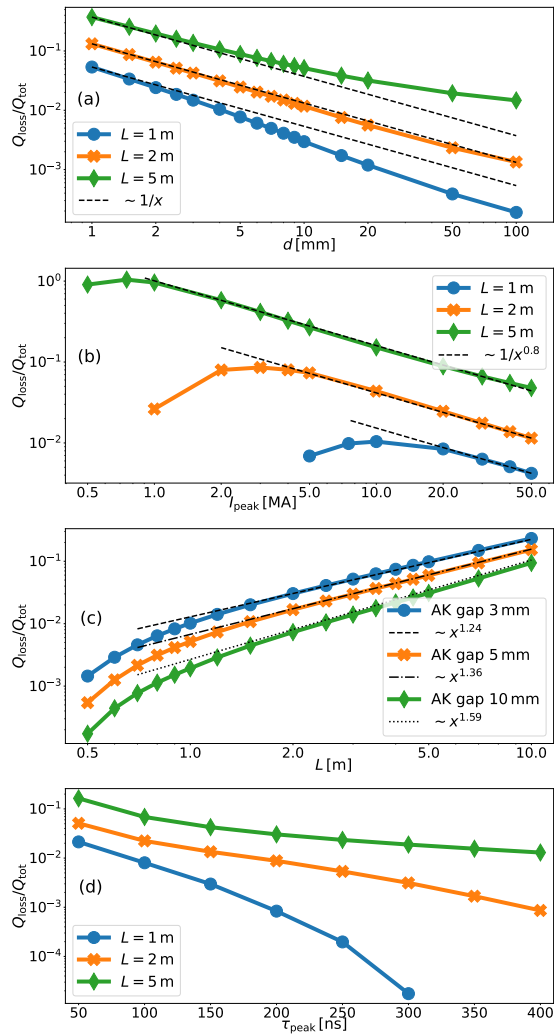


FIG. 6. Scaling studies of loss charge. Panel (a): Scaling with AK gap, d , for fixed $I_{\text{peak}} = 20$ MA and $\tau_{\text{peak}} = 100$ ns. Panel (b): Scaling with peak current, I_{peak} , for a fixed AK gap, $d = 5$ mm and $\tau_{\text{peak}} = 100$ ns. Panel (c): Scaling with pulse length, τ_{peak} , for a fixed $I_{\text{peak}} = 20$ MA and AK gap, $d = 5$ mm. Panel (d): Scaling with MITL length, L , for a fixed $I_{\text{peak}} = 20$ MA and $\tau_{\text{peak}} = 100$ ns.

The next Fig. 6 (b) shows how MITL losses scale with peak current, I_{peak} , for a given fixed MITL length, pulse length $\tau_{\text{peak}} = 100$ ns, and $d = 5$ mm. The fractional losses exhibit a maximum at a certain value of peak current, vanish for small currents, and decrease for large peak currents. We can understand this behavior in the following way. On the one hand, smaller peak currents have smaller losses due to the shorter time of uninsulated SCL emission: regardless of the drive current amplitude, SCL emission turns on only after exceeding some threshold value, say $E_{\text{th}} = 24$ MV/m in our case. If the peak current is too low, that threshold value cannot be exceeded since for a fixed τ_{peak} , $E \sim I_{\text{peak}}$. On the other hand, large peak currents induce larger diamagnetic effects, which lower the losses. Obviously, peak currents

around the maximum of the curve should be avoided in MITL designs. A common scaling of MITL losses for large peak currents emerges in the form of $\sim 1/x^{0.8}$, which we leave as an empirical observation.

In Fig. 6 (c) we show the scaling of MITL losses with MITL length for fixed $I_{\text{peak}} = 20$ MA and $\tau_{\text{peak}} = 100$ ns, for three different AK gap sizes. At shorter lengths, the current losses drop due to the decreased time of uninsulated SCL emission. In the limit of (infinitely) short MITLs, we converge to the losses predicted by the Child-Langmuir law in vacuum fields (not shown). Similarly, we can understand the increased current losses in longer MITLs as increased time of uninsulated SCL emission. Recall that magnetic insulation cannot happen in pure TEM fields, i.e., for which $E = cB$. Electrons perform a figure-8 motion in such fields, not a cyclotron motion, and our estimates have shown that the size of such an orbit for typical fields of interest is much larger than the AK gap; this means such electrons are uninsulated. Magnetic insulation can occur *after reflection* from the load because the relation $E = cB$ no longer holds due to the interference (superposition) of the incoming and outgoing waves. In longer MITLs, reflection takes longer to happen, hence, the increased losses. For the range of lengths shown, we again uncover an empirical scaling law for large L , which, however, differs for the different gap sizes.

It is worth commenting on the losses in *infinitely long* MITLs. Although magnetic insulation never occurs in such MITLs, current losses are still limited by two effects: (i) the Child-Langmuir law limits the amount of current crossing the AK gap; and (ii) the non-local diamagnetic effects further lower the amount of loss current; in fact, these latter effects are maximally manifested in this case.

The last Fig. 6 (d) shows scaling of MITL losses with pulse duration. This scaling is the strongest of the four examples shown in the figure, showing exponential or super-exponential dependence (notice the semi-log scale of the plot). The losses for the 1 m-long MITL fall to zero past about $\tau_{\text{peak}} \gtrsim 300$ ns. These losses can also be understood in terms of ununsulation time, which is longer for longer MITLs. Another intuitive understanding can be given by the relation $E \sim dI/dt$, showing lower fields for longer pulse lengths. (This relation strictly applies only in the infinitely short MITL or equivalently, the limit of $c \rightarrow \infty$, see also Ref. [38]). No common empirical scaling law emerges in this case.

V. MAGNETIC INSULATION MODEL

The magnetic insulation model is a common ingredient in several major circuit element models. Since it is also used in our 1D model, it deserves special attention.

The issue at hand is the value of the SCL current crossing the AK gap as a function of magnetic field magnitude. A theoretical value of the critical magnetic field (also called the Hull field), at which complete insulation

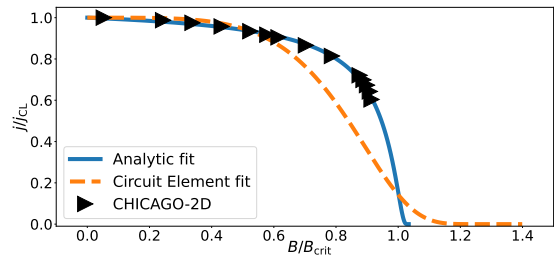


FIG. 7. Comparison of the Hull curve used in our 1D model, ‘Analytic fit’, and the Hull curve used presently in circuit element codes, ‘Circuit Element fit’. CHICAGO 2D PIC simulations are shown with black triangles.

occurs, was derived by Lovelace and Ott [7]. The expression they derived depends on the value of the potential (difference), V_0 , [cf. Eqs. (12) and (13)] and is given by

$$B_{\text{crit}} = \frac{mc}{ed} \sqrt{\left(\frac{eV_0}{mc^2}\right)^2 + \frac{2eV_0}{mc^2}}. \quad (19)$$

The expression (19) was experimentally tested by Orzechowski and Bekefi [39] who found that magnetic insulation occurred mostly in agreement with Eq. (19) but SCL current did not sharply drop to zero at the Hull magnetic field value; instead, it had a “spillover.” They constructed a curve by normalizing the measured current to $V_0^{3/2}$ (from the Child-Langmuir law) and the magnetic field to the critical magnetic field, (19). We follow Ref. [40] and normalize the loss current to the Child-Langmuir current. Since the expression for the Child-Langmuir current folds in the particular geometry, one can think of such a curve as universal. We refer to this curve as the Hull curve.

As CEM is concerned in regards to predicting SCL current losses in MITLs, we note that major codes, such as BERTHA and SCREAMER, use the curve plotted in Fig. 7 of Ref. [40], labeled “Original SCREAMER.” Reference [40] also proposes a revised version of the curve, however, such revision does not appear to have been widely implemented [41]. We refer to the curve “Original SCREAMER” from Ref. [40] more generally as the “Circuit Element fit.” This curve is shown as a dashed line³ in Fig. 7. Reference [40] additionally states that the Hull curve has been constructed from 3D PIC simulations. We attempted to replicate the curve using 2D PIC simulations with CHICAGO and found that our results did not agree with the Circuit Element fit curve, as indicated by the black triangles in Fig. 7.

The source of disagreement is worth discussing. One can see that our simulation data stops at about $B/B_{\text{crit}} = 0.91$. The reason behind this is that as we approached the Hull magnetic field, the electron layer transitioned from

³ Our fit of that curve is based on the image from Ref. [40].

stable and steady-state to unstable. In an unstable layer, the current collected by the anode as well as the electric field acquire oscillatory behavior (the magnetic field stays nearly constant since it is externally imposed). In such a system, averaged values are difficult to obtain due to the randomness in the oscillations. Even if averaged values were possible to reliably obtain, they would not be representative of a steady-state system, upon which assumption both the Child-Langmuir law and Hull magnetic field calculations are based. However, knowing an accurate value of V_0 is crucially important since both the Child-Langmuir current and the critical magnetic field strongly depend on it, as seen from Eqs.(12) and (19). These two quantities are being used to normalize the measured current and magnetic field, and because of that, any uncertainty in V_0 translates into uncertainty in the normalized quantities on the Hull curve. Our experience has shown that near cutoff, small uncertainty in V_0 can easily place a point on either side of the theoretical Hull field.

Apart from the uncertainty associated with the value of V_0 , our PIC simulations also show the “spillover” effect and loss of a sharp insulating boundary. These observations have led us to revisit the *interpretation* of the experimental results in Ref. [39]. In that reference, it was hypothesized that some process, not characterized by the authors, produced “hot tail” electrons that contributed to smearing of the sharp theoretical boundary. The authors detected radiation when the magnetic field strength exceeded the Hull field and no such radiation for lower magnetic fields, which they also correlated with the onset of an instability in the system. To our knowledge, the precise mechanism for such “hot electrons” has not been identified in the literature to date. Here we suggest another possible instability leading to the loss of a sharp insulating boundary, in agreement with our PIC simulations. Namely, we propose that the electron layer loses stability due to a velocity shear type instability in crossed field devices, such as diocotron, magnetron, etc. In such an unstable layer, our observations show the formation of large-scale vortical structures that move in a stochastic way throughout the system (largely because of $\mathbf{E} \times \mathbf{B}$ drift), leading to stochastic oscillatory behavior in all quantities within the AK gap, including in the conducting current. Such mechanism results in a loss current beyond the Hull field but does not necessarily produce a population of hot electrons. Ultimately, to be able to unambiguously identify the precise instability, a further study beyond the scope of this work is necessary.

The stability properties of a parapotential magnetized electron layer have been discussed in the past [28, 42, 43]. While these properties depend on the layer’s spatial profile, of equal importance is whether and how this profile may in practice (experiment) be achieved. Many factors make this problem very complex, however, for relevant to Z parameters, even the simplest constant profile electron layer is never strictly stable, something recently emphasized in Ref. [36]. An attempt to create a stable electron layer by the authors of Ref. [44] was also not success-

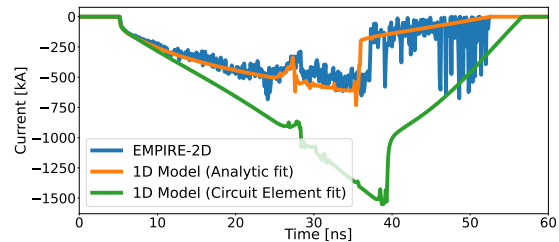


FIG. 8. Comparison of current losses in a 5 m long MITL with $I_{\text{peak}} = 20$ MA, $\tau_{\text{peak}} = 100$ ns, AK gap, $d = 5$ mm. The Circuit Element fit overpredicts EMPIRE 2D PIC result by about a factor of 3 while the Analytic fit is in excellent agreement with it.

ful. We believe that in order to properly understand the loss of a sharp insulating boundary, a theory of current transport across an AK gap in unsteady flows must be developed.

Let us discuss the choice and analytic representation of our Hull curve. Our fit is based on the formula

$$y(x) = \begin{cases} e^{-a|x|^\alpha/|x-b|}, & x \leq 0 < b \\ 0, & x \geq b \end{cases} \quad (20)$$

with positive a , b , and α . Our Analytic fit Hull curve is obtained for values $a = 0.065$, $b \in [1.03, 1.04]$, and $\alpha = 1$; the Circuit Element fit is obtained for $a = 0.78$, $b = 1.4$, and $\alpha = 4$. The notable feature here is that our analytic fit has a much smaller range outside the critical magnetic field, by only about 3–4%, compared to about 40% for the Circuit Element fit.

Since our PIC simulations were not successful in constructing the entire Hull curve, we have fitted the parameters in Eq. (20) from PIC simulations of current loss in MITLs of various geometrical dimensions. In particular, long MITLs have an amplifying effect on small variations in parameter values. Fig. 8 shows a simulation of current loss in a 5 m long MITL ($I_{\text{peak}} = 20$ MA, $\tau_{\text{peak}} = 100$ ns, AK gap, $d = 5$ mm), which illustrates the difference in the predictions using the two different fits from Fig. 7. Clearly, the Circuit Element fit greatly overpredicts current losses, by a factor of about 3. (We have confirmed this result also by a direct simulation with BERTHA, not shown here.) Conversely, the details of the Hull curve in shorter MITLs in the length range $\lesssim 2$ m do not manifest significant discrepancy with PIC simulations and both fits produce acceptable predictions.

One last remark in this section is that a “spillover” Hull curve acts as a low pass filter. Looking back at Fig. 5, we notice that the 1D model contains a certain amount of small scale temporal oscillations. Such oscillations are not PIC noise since the 1D model is a (cold) fluid model. Comparing now the simulation with the Circuit Element fit in Fig. 8, we see a noticeably smoother curve. This is not to imply that removing the small scale oscillations is unphysical, rather, that it is possible that certain physical oscillations may unintentionally be filtered out.

VI. TEMPERATURE RISE DUE TO ELECTRON IMPACT

Temperature rise due to electron impact can be calculated within our 1D model as a diagnostic. Electrons impacting the anode deliver a certain amount of energy to the surface, contributing to temperature increase. For the time scale of our current pulses, a negligible amount of heat is dissipated within the metal volume, therefore, our calculation simply accumulates the electron energy and temperature impacted to the anode surface.

We use the NIST stopping power tables for electrons in metals, dK/dx [45]; or for certain metals, we prefer to use an analytic expression that gives the extra information in the low energy range [46]. First, the electron flux to the anode is directly related to the electron current:

$$F(z, t) = \left| \frac{j_x(z, t)}{e} \right|. \quad (21)$$

The temperature increase due to electron impact in time Δt at time t_k is then

$$\Delta T_k = \Delta T(z, t_k) = \frac{M_{\text{mol}} |dK/dx| \int_{t_k}^{t_k + \Delta t} F(z, t) dt}{\rho C_V} \frac{1}{\cos \theta_i}, \quad (22)$$

where M_{mol} is the molar mass of the metal, ρ is the mass density, C_V is the heat capacitance at constant volume, and θ_i is the electron angle of incidence measured from the normal to the surface (see also Ref. [16]). The total temperature increase is the sum over all time steps, $N_{\text{ins}} = t_{\text{ins}}/\Delta t$, until complete magnetic insulation is achieved,

$$\Delta T^{\text{tot}}(z) = \sum_{k=0}^{N_{\text{ins}}} \Delta T_k(z, t_k). \quad (23)$$

The only extra information necessary to calculate the temperature rise is the angle of incidence, which can be calculated as follows. Using the steady-state relations for conservation of the z -component of canonical momentum and the energy balance in Cartesian geometry [7, 47], we have

$$mv_z(x)\gamma(x) - eA_z(x) = \text{const.} = 0, \quad (24)$$

$$mc^2 [\gamma(x) - 1] - eV(x) = 0, \quad (25)$$

where the relativistic factor is defined as usual, $\gamma = [1 - (v_x^2 + v_z^2)/c^2]^{-1/2}$, with electron velocities v_x and v_z . We note that the vector potential in Eq. (24) is *not* the same as in Eq. (2). For a constant magnetic field in the y -direction, we can choose $\mathbf{A} = (0, 0, -B_0x)$,⁴ which

gives $B_y = (\nabla \times \mathbf{A})_y = B_0$. We can calculate $\cos \theta_i$ as

$$\cos \theta_i = \frac{v_x}{\sqrt{v_x^2 + v_z^2}}. \quad (26)$$

Hereafter we calculate all quantities at the anode, $x = d$. It is straightforward to find from (24) and the definition of γ

$$v_z = \frac{e}{m} \frac{B_y d}{\gamma}, \quad \sqrt{v_x^2 + v_z^2} = \frac{c\sqrt{\gamma^2 - 1}}{\gamma}, \quad (27)$$

from which

$$\cos \theta_i(z, t) = \sqrt{1 - \frac{1}{\gamma^2 - 1} \left(\frac{eB_y(z, t)d}{mc} \right)^2}. \quad (28)$$

Upon using Eq. (25), it is easy to recognize that setting the radical expression in Eq. (28) to zero, i.e., $\gamma^2 - 1 - (eB_y d/mc)^2 = 0$, amounts to precisely the Hull condition⁵ (19). This means that the angle of incidence (28) is undefined at insulation (by Lovelace and Ott) as well as for larger values of the magnetic field, for which the expression under the square root becomes negative. In other words, using a Hull curve with a “spillover” is incompatible with the so outlined method of calculating the temperature. The simplest approach to resolving this incompatibility is to neglect temperature contributions at locations where $B_y \geq B_{\text{crit}}$. This simple solution is acceptable for two reasons. First, we have seen from the Hull curve in Fig. 7 that the electron flux, which is proportional to the current, significantly drops near B_{crit} , and so does its contribution to the temperature rise. And second, the neglected range of magnetic fields is only a small fraction of 3–4% of the total range for our Analytic fit. Our practical experience has confirmed that temperature doesn’t noticeably increase at locations near magnetic insulation.

As a verification of this approach, Fig. 9 shows the temperature rise calculated from data from our 1D model and from CHICAGO 2D PIC, for aluminum metal initially at 300 K. The simulation setup is the same as in Fig. 4. To avoid small differences due to algorithmic implementation details, we use CHICAGO’s output quantities of current density and kinetic energy near the anode (quantities from particles information accumulated to the grid) to perform the calculations leading to Eq. (23). We notice that the overall agreement between the two models is excellent. This implies also that not only do both components of the current density agree very well (we have not shown z -components from either model) but so do the kinetic energies. The slight disagreement in the range of 20–30 cm at $t = 9$ ns (top panel) is due to the slight temporal delay of the PIC pulse compared to the 1D model,

⁴ One can easily extend this condition to spatially uniform, time-dependent electric fields by choosing $\mathbf{A} = (A_x(t), 0, -B_0x)$, giving $E_x(t) = -dA_x(t)/dt$.

⁵ The Hull condition can be derived from the same equations by setting $v_x = 0$ at $x = d$, i.e., the condition that electrons do not reach the anode.

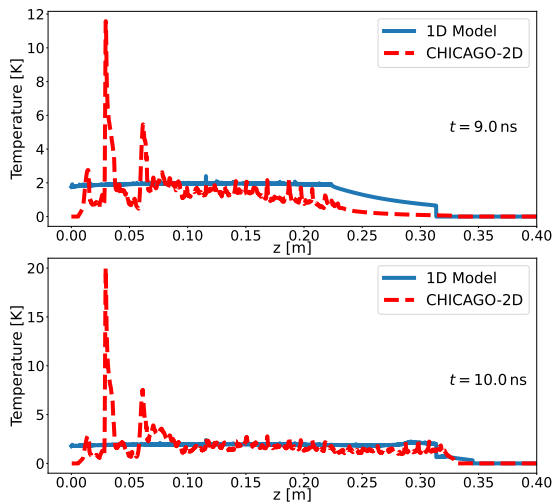


FIG. 9. Comparison of temperature increase at $t = 9$ ns (top) and 10 ns (bottom) between the 1D model and CHICAGO 2D PIC simulations, for $I_{\text{peak}} = 20$ MA, $\tau_{\text{peak}} = 100$ ns, AK gap, $d = 5$ mm, and $L = 1$ m.

see Fig. 4 (bottom panel); however, just 1 ns later, at 10 ns (bottom panel) no such disagreement is seen (the current loss pulses have caught up to one another). Since the temperature calculation is cumulative, such temporal offsets would not affect the final temperature increase.

The obvious question concerns the large temperature oscillations in the PIC simulation in the first ~ 10 cm of the MITL. These oscillations correspond to the current (and flux) oscillations in Fig. 4, which we believe to be a numerical artifact of the SCL emission algorithm in PIC, as discussed in Ref. [36].

VII. CONCLUSIONS

In this work we have discussed MITL losses in a strongly time-dependent setting. A major effect that helps dramatically reduce current losses in long MITLs is that of the diamagnetic, non-local cumulative electromagnetic effect of SCL currents. In short MITLs these effects diminish and in the limit vanish.

A new 1D electromagnetic model is developed that performs six to seven orders of magnitude more efficiently than 2D PIC computations. The model has been verified against 2D PIC simulations of parallel plate Cartesian and straight coaxial MITL with azimuthal symmetry. It allows for efficient navigation of the large MITL design parameter space. A number of scaling studies have been performed, helping to understand and minimize MITL losses. A temperature diagnostic within the 1D model is easy to implement, based on the available information from the fields and currents. Agreement with the temperature calculations from PIC data further verifies that the 1D model accurately predicts kinetic energies as well.

A revised magnetic insulation model is proposed in the

form a Hull curve, partly informed by PIC simulations and partly by fitting PIC simulation data. It is found that close to magnetic insulation, the electron layer between the anode and cathode becomes unstable and prevents the computation of the complete Hull curve. Major circuit element codes using a previously computed Hull curve tend to overpredict current losses in long MITLs but implementation of our revised Hull curve should not present difficulty.

It is proposed that previous experimental observations by Orzechowski and Bekefi of non-zero loss current beyond the theoretical critical magnetic field by Lovelace and Ott is due to the electron layer losing stability, which also fits within the physics picture based on PIC simulations. This hypothesis still needs experimental confirmation.

ACKNOWLEDGMENTS

The authors acknowledge useful feedback and discussions with Greg Frye, Josh Leckbee, Keith Matzen, Kate Bell, Brian Hutsel, David Sirajuddin and Christopher Jennings from SNL. This work was funded by Laboratory Directed Research and Development grant No. 229292. Sandia National Laboratories is a multimission laboratory managed and operated by National Technology & Engineering Solutions of Sandia, LLC, a wholly owned subsidiary of Honeywell International Inc., for the U.S. Department of Energy's National Nuclear Security Administration under contract DE-NA0003525. This paper describes objective technical results and analysis. Any subjective views or opinions that might be expressed in the paper do not necessarily represent the views of the U.S. Department of Energy or the United States Government.

Appendix A COAXIAL GEOMETRY

A straight coaxial MITL can be simulated within the 1D model with minor adjustments. Calculations in the cylindrical geometry (r, θ, z) with azimuthal symmetry (in the θ -direction) closely parallel those in Cartesian. For our purposes, invoking the small AK gap approximation (A-i) allows to consider the radius of the coaxial MITL as only a parameter. Within the error of that approximation, that radius can be chosen as either the inner or the outer. Our choice of cathode is typically the inner electrode, while the anode is the outer one. Accordingly, we choose the outer radius when comparing fields and current densities at the anode.

We can make the following adjustments in the 1D model. Denoting the radius of the coaxial MITL by R , we adjust the current density in the wave equation (2) to

$$j_x \longrightarrow j_r = \frac{j_x}{2\pi R} \quad (29)$$

The electric and magnetic fields follow from the same Eqs. (6), (7) but with the correction

$$E_x \longrightarrow \frac{E_x}{2\pi R}, \quad B_\theta = \frac{E_r}{c}. \quad (30)$$

Intuitively, in the small AK gap approximation the

coaxial MITL is expected to behave as Cartesian. Our simulations have confirmed that such an adjusted “coaxial” 1D model also has excellent agreement with both CHICAGO 2D PIC simulations (in the (r, z) coordinates) and EMPIRE PIC simulations of a thin 3D wedge.

-
- [1] D. B. Sinars et al. Review of pulsed power-driven high energy density physics research on Z at Sandia. *Phys. Plasmas*, 27(7):070501, July 2020.
- [2] R. D. McBride, W. A. Stygar, M. E. Cuneo, D. B. Sinars, M. G. Mazarakis, and J. J. Leckbee et al. A primer on pulsed power and linear transformer drivers for high energy density physics applications. *IEEE Transactions on Plasma Science*, 46(11):3928–3967, 2018.
- [3] W. A. Stygar, T. J. Awe, J. E. Bailey, N. L. Bennett, E. W. Breden, and E. M. Campbell et al. Conceptual designs of two petawatt-class pulsed-power accelerators for high-energy-density-physics experiments. *Phys. Rev. ST Accel. Beams*, 18:110401, Nov 2015.
- [4] E. I. Baranchikov, A. V. Gordeev, Yu. V. Koba, V. D. Korolev, and V. S. et al. Pen’kina. Transfer and focusing of high-current relativistic electron beams onto a target. *IAEA, Vienna*, 1:185–203, 1977.
- [5] Marco S. Di Capua and Donald G. Pellinen. Propagation of power pulses in magnetically insulated vacuum transmission lines. *J. Appl. Phys.*, 50(5):3713–3720, 1979. Publisher: American Institute of Physics.
- [6] J. P. VanDevender. Long self-magnetically insulated power transport experiments. *J. Appl. Phys.*, 50(6):3928–3934, June 1979. Publisher: American Institute of Physics.
- [7] R. V. Lovelace and E. Ott. Theory of magnetic insulation. *Phys. Fluids*, 17(6):1263–1268, June 1974. Publisher: American Institute of Physics.
- [8] J. M. Creedon. Relativistic brillouin flow in the high ν/γ diode. *J. Appl. Phys.*, 46:2946, 1975.
- [9] Marco S. Di Capua. Magnetic Insulation. *IEEE Transactions on Plasma Science*, 11(3):205–215, September 1983. Conference Name: IEEE Transactions on Plasma Science.
- [10] C. W. Mendel Jr., D. B. Seidl, and S. A. Slutz. A general theory of magnetically insulated electron flow. *Phys. Fluids*, 26:3628, 1983.
- [11] P. F. Ottinger and J. W. Schumer. Magnetically insulated ion flow theory. *Phys. Plasmas*, 13:063101, 2006.
- [12] T.D. Pointon, W.L. Langtson, and M.S. Savage. Particle-in-Cell Simulations of the Magnetically Insulated Transmission Lines and Post-Hole Convolute of ZR, 2007.
- [13] T. D. Pointon and D. B. Seidel. Current loss in the vacuum section of the refurbished Z accelerator. In *2009 IEEE Pulsed Power Conference*, pages 1159–1164, June 2009. ISSN: 2158-4923.
- [14] P. F. Ottinger and J. W. Schumer. Rescaling of equilibrium magnetically insulated flow theory based on results from particle-in-cell simulations. *Phys. Plasmas*, 13(6):063109, June 2006. Publisher: American Institute of Physics.
- [15] D. R. Welch, N. Bennett, T. C. Genoni, D. V. Rose, C. Thoma, C. Miller, and W. A. Stygar. Electrode contaminant plasma effects in 10^7 -A Z pinch accelerators. *Phys. Rev. Accel. Beams*, 22(7):070401, July 2019. Publisher: American Physical Society.
- [16] N. Bennett, D. R. Welch, C. A. Jennings, E. Yu, B. T. Hutsel, G. Laity, J. K. Moore, D. V. Rose, K. Peterson, and M. E. Cuneo. Current transport and loss mechanisms in the Z accelerator. *Phys. Rev. Accel. Beams*, 22(12):120401, December 2019.
- [17] D. R. Welch, N. Bennett, T. C. Genoni, C. Thoma, and D. V. Rose. Fast hybrid particle-in-cell technique for pulsed-power accelerators. *Phys. Rev. Accel. Beams*, 23(11):110401, November 2020. Publisher: American Physical Society.
- [18] C. K. Birdsall and A. B. Langdon. *Plasma Physics via Computer Simulation*. Series in Plasma Physics. Taylor & Francis, New York, 1st edition, 2005.
- [19] R. W. Hockney and J. W. Eastwood. *Computer Simulation Using Particles*. CRC Press, March 2021.
- [20] D. D. Hinshelwood. BERTHA - A Versatile Transmission Line and Circuit Code. MRL Memorandum Report 5195, Naval Research Laboratory, Alexandria, VA, 1983. Section: Technical Reports.
- [21] George A. Huttlin and Alvars J. Lelis. TLINES: A Computer Program for Circuits of Transmission Lines. Technical Report AD-A139596, Harry Diamond Labs, Adelphi, MD, December 1983.
- [22] W.N. Weseloh. Tlcode - a transmission line code for pulsed power design. In *7th Pulsed Power Conference*, pages 989–992, June 1989.
- [23] C. Harjes, J. Elizondo, K. Struve, L. Bennett, D. Johnson, and B. Shoup. Circuit modeling for ZR. In *Digest of Technical Papers. PPC-2003. 14th IEEE International Pulsed Power Conference (IEEE Cat. No.03CH37472)*, volume 2, pages 917–920 Vol.2, June 2003.
- [24] R. B. Spielman and D. B. Reisman. On the design of magnetically insulated transmission lines for z-pinch loads. *Matter Radiat. Extremes*, 4(2):027402, March 2019.
- [25] C. D. Child. Discharge From Hot CaO. *Phys. Rev. (Series I)*, 32(5):492–511, May 1911. Publisher: American Physical Society.
- [26] I. Langmuir. The Effect of Space Charge and Residual Gases on Thermionic Currents in High Vacuum. *Phys. Rev.*, 2(6):450–486, December 1913. Publisher: American Physical Society.
- [27] V. S. Vladimirov. *Equations of mathematical physics*. Mir Publishers, first edition edition, January 1984.
- [28] Ronald C. Davidson. *Physics Of Nonneutral Plasmas*. World Scientific Publishing Company, October 2001. Google-Books-ID: 5s02DwAAQBAJ.

- [29] Matthew T. Bettencourt, A. S. Brown Dominic, Keith, Keith L. Cartwright, Eric C. Cyr, A. Glusa Christian, T. Lin Paul, Stan G. Moore Moore, Duncan A. O. McGregor McGregor, Roger P. Pawlowski, Edward G. Phillips, Nathan V. Roberts, Steven A. Wright Wright, Satheesh Maheswaran, John P. Jones, and Stephen A. Jarvis. EMPIRE-PIC: A Performance Portable Unstructured Particle-in-Cell Code. *Communications in Computational Physics*, 30(4):1232–1268, 2021.
- [30] D. R. Welch, D. V. Rose, R. E. Clark, T. C. Genoni, and T. P. Hughes. Implementation of a non-iterative implicit electromagnetic field solver for dense plasma simulation. *Computer Physics Communications*, 164(1):183–188, December 2004.
- [31] D. R. Welch, T. C. Genoni, R. E. Clark, and D. V. Rose. Adaptive particle management in a particle-in-cell code. *Journal of Computational Physics*, 227(1):143–155, November 2007.
- [32] T. C. Genoni, R. E. Clark, and D. R. Welch. A Fast Implicit Algorithm for Highly Magnetized Charged Particle Motion. *The Open Plasma Physics Journal*, 3(1), April 2010.
- [33] T. D. Pointon. Slanted conducting boundaries and field emission of particles in an electromagnetic particle simulation code. *Journal of Computational Physics*, 96(1):143–162, September 1991.
- [34] J. J. Watrous, J. W. Luginsland, and G. E. Sasser. An improved space-charge-limited emission algorithm for use in particle-in-cell codes. *Phys. Plasmas*, 8(1):289–296, January 2001. Publisher: American Institute of Physics.
- [35] J. W. Luginsland, Y. Y. Lau, R. J. Umstattd, and J. J. Watrous. Beyond the Child–Langmuir law: A review of recent results on multidimensional space-charge-limited flow. *Phys. Plasmas*, 9(5):2371–2376, May 2002.
- [36] E. G. Evstatiev and M. H. Hess. Efficient kinetic particle simulations of space charge limited emission in magnetically insulated transmission lines using reduced physics models. *Phys. Rev. Accel. Beams*, 26(9):090403, September 2023. Publisher: American Physical Society.
- [37] K. D. Bergeron. Equivalent circuit approach to long magnetically insulated transmission lines. *J. Appl. Phys.*, 48(7):3065–3069, 1977.
- [38] M. H. Hess and E. G. Evstatiev. Electron Dynamics Within a MITL Containing a Load. *IEEE Trans. Plasma Sci.*, 49(11):3398–3409, November 2021. Conference Name: IEEE Transactions on Plasma Science.
- [39] T. J. Orzechowski and G. Bekefi. Current flow in a high-voltage diode subjected to a crossed magnetic field. *Phys. Fluids*, 19(1):43–51, January 1976.
- [40] J. Pace VanDevender, Timothy D. Pointon, David B. Seidel, Kenneth W. Struve, Christopher Jennings, Bryan V. Oliver, and Larry X. Schneider. Requirements for self-magnetically insulated transmission lines. *Phys. Rev. ST Accel. Beams*, 18(3):030401, March 2015. Publisher: American Physical Society.
- [41] R. B. Spielman. Private communication.
- [42] O. Buneman, R. H. Levy, and L. M. Linson. Stability of Crossed-Field Electron Beams. *J. Appl. Phys.*, 37(8):3203–3222, 1966.
- [43] Ronald C. Davidson, Hei-Wai Chan, Chiping Chen, and Steven Lund. Equilibrium and stability properties of intense non-neutral electron flow. *Rev. Mod. Phys.*, 63(2):341–374, April 1991. Publisher: American Physical Society.
- [44] K. D. Bergeron and J. W. Poukey. Beam stability and current loss in magnetic insulation. *Journal of Applied Physics*, 50(7):4996–5000, July 1979. Publisher: American Institute of Physics.
- [45] M. Berger, J. Coursey, and M. Zucker. ESTAR, PSTAR, and ASTAR: Computer programs for calculating stopping-power and range tables for electrons, protons, and helium ions (version 1.21), 1999-01-01 1999.
- [46] H. T. Nguyen-Truong. Modified Bethe formula for low-energy electron stopping power without fitting parameters. *Ultramicroscopy*, 149:26–33, February 2015.
- [47] K. D. Bergeron and J. W. Poukey. Relativistic space-charge flow in a magnetic field. *Appl. Phys. Lett.*, 27(2):58–60, July 1975. Publisher: American Institute of Physics.